applied sciences

MDPI

Article

Transport Percolation Diagram of Composite Medium Predicted by Microscopically Calibrated Lattice Model and Data-Driven Analysis

Shaohua Chen [1], Haoyu Wang [1] and Nuo Xu [2,*]

[1] College of Energy and Power Engineering, Nanjing University of Aeronautics and Astronautics, Nanjing 210016, China; csh990729@163.com (S.C.); 18609961260@163.com (H.W.)
[2] College of Mechanics and Engineering Science, Hohai University, Nanjing 211100, China
* Correspondence: xunuo1994@hhu.edu.cn

Abstract

Electrical conduction and thermal conduction in homogeneous composites are often considered analogous macroscopic transport phenomena due to the identical mathematical formulation of Ohm's law and Fourier's law. However, this analogy breaks down in multiphase composites, where their behaviors can differ markedly. Experimental evidence shows that electrical percolation is often readily observed, whereas thermal percolation remains elusive and even debated. To address this, we develop a simplified yet carefully calibrated lattice model to efficiently simulate the macroscopic transport behavior of composite material and generate large datasets across a wide transport parameter space. Data-driven analysis reveals a boundary separating percolating and non-percolating regimes, leading to a transport percolation diagram that distinguishes "easy" and "hard" percolation. Additionally, a numerical singularity associated with interfacial area is identified in the percolation-allowed regime, indicating that the occurrence of numerical instability might be used as the criterion for the presence of transport percolation.

Keywords: transport percolation; electrical conduction; thermal conduction; data-driven analysis; multiphase composite

1. Introduction

As two ubiquitous transport phenomena in materials, thermal conduction and electrical conduction arise from fundamentally different microscopic mechanisms. Thermal conduction is mediated by energy carriers such as phonons, electrons, or molecular motion, depending on the material, whereas electrical conduction is governed by the drift of mobile charge carriers under an electric field. Nevertheless, there seems to be a mathematical analogy between them. The relevant physical quantities correspond one-to-one: heat flux $\boldsymbol{q}$ and current density $\boldsymbol{j}$, temperature T and electric potential V, and thermal conductivity κ and electrical conductivity σ. Moreover, their steady states are described by formally identical relations, namely Fourier's law ($\boldsymbol{q} = -\kappa\nabla T$) and Ohm's law ($\boldsymbol{j} = -\sigma\nabla V$). Despite these parallels, the two processes can exhibit markedly different behavior in practice, particularly in heterogeneous multiphase materials, where transport percolation provides a notable example [1,2].

For a two-phase material with a matrix and a second-phase filler particle, percolation theory predicts that a globally spanning cluster of the second phase emerges once its fraction exceeds the percolation threshold. Such topological percolation of the second

Academic Editor: Young-Wook Chang

Received: 4 July 2026
Revised: 23 July 2026
Accepted: 23 July 2026
Published: 6 August 2026

phase might strongly impact the physical properties of the material and usually leads to an associated percolation transition in the macroscopic transport properties, such as electrical and thermal conductivities [3,4]. Taking the graphene-reinforced polymer composite as an example, the electrical conductivity of a polymer is commonly on the order of $10^{-10}\ S \cdot m^{-1}$, while that of the graphene is on the order of $10^{6}\ S \cdot m^{-1}$. Once the graphene phase reaches its topological percolation threshold, the electrical conductivity of the composite can exhibit an increase of several orders of magnitude [5–9]. Meanwhile, the thermal conductivities of polymer and graphene are usually on the orders of $0.1\ W \cdot m^{-1} \cdot K^{-1}$ and $10^{3}\ W \cdot m^{-1} \cdot K^{-1}$, but the existence of thermal percolation in graphene-reinforced polymer composites is still under debate [10]. Although such distinction is mainly reported in composites consisting of carbon-based conductive fillers, such as graphene and carbon nanotubes, embedded in polymer matrices, including PA-6, polypropylene (PP), and polymethyl methacrylate (PMMA), these systems are nevertheless representative of a broad class of composites composed of electrically insulating matrices reinforced with highly conductive fillers.

Some researchers believe that the distinction is mainly attributed to the difference between the transport properties of the matrix and the second phase. As pointed out by Lasance [11], the electrical conductivity of an electrical conductor can be as high as 20 orders of magnitude higher than that of an electrical insulator, while the thermal conductivity of a thermal conductor is only a few orders of magnitude higher than that of a thermal insulator. Therefore, it is erroneous to draw a practical analogy between thermal conduction and electrical conduction. Similarly, based on the difference between the transport properties of the matrix and the second phase, Sarikhani et al. categorize the macroscopic transport behavior of multiphase materials into different types, i.e., the conductor–superconductor type, the insulator–conductor type, and the poor conductor–good conductor type [12]. Forero-Sandoval et al. provide a comprehensive perspective on electrical and thermal percolation in two-phase materials, reviewing experimental observations and theoretical frameworks [13]. These views hold that the larger the difference between the transport properties of the matrix and the second phase, the more likely the emergence of transport percolation. However, insightful as they are, some critical questions remain unresolved. For example, what is the quantitative criterion that determines whether a given material system will exhibit transport percolation? Can a unified predictive framework be developed that connects nanoscale interface properties to the emergence or absence of percolation transitions?

In this work, we address these gaps by combining microscopically validated lattice models, high-throughput finite element simulations, and data-driven analysis to establish a qualitative percolation diagram for the macroscopic transport behavior in multiphase media. We make four key contributions: (i) We develop a microscopically inspired lattice model validated against non-equilibrium molecular dynamics simulations that captures the essential physics of matrix, filler, and interfacial transport with explicit parameterization of interfacial transport efficiency. (ii) Through systematic parametric exploration spanning five orders of magnitude in interfacial and contact transport parameters, we identify two dimensionless parameters as the critical discriminator between percolation-allowed and percolation-prohibited regimes. (iii) We construct a diagram in the dimensionless parametric space that provides qualitative phase boundaries and enables a priori prediction of whether transport percolation will emerge in a given material system. (iv) We identify a numerical singularity present in both FEM simulation and molecular dynamics simulation that apparently violates the macroscopic governing differential equation, which signifies the shortcomings of current computational methods when dealing with transport simulations involving extremely different transport parameters.

The remainder of this paper is organized as follows. Section 2 describes the development and validation of the microscopically inspired lattice model against molecular dynamics simulations. Section 3 presents the high-throughput parametric study, data-driven transport percolation diagram discovery, and analysis of the percolation transition mechanism. Section 4 discusses the numerical instabilities in transport percolation, which can be observed in both the finite element method (FEM) and molecular dynamics (MD). Section 5 concludes with a summary of key findings.

2. A Microscopically Inspired Lattice Model for Macroscopic Transport Behavior

Let us consider a specific case of multiphase composite material, the graphene-reinforced polyamide-6 (PA-6) composite. Graphene has ultrahigh electrical conductivity and thermal conductivity, while the polymer matrix is usually an insulator in terms of both electrical and thermal conductions [14]. Although experiments show that the existence of thermal percolation in this composite system is ambiguous, our previous MD simulation work has proven that thermal percolation is possible in principle [15]. Therefore, the graphene-reinforced polymer composite is an ideal example for the study of transport percolation. Figure 1a demonstrates a quasi-2D full-atom configuration of the graphene–polymer composite. Each graphene sheet is oriented either horizontally or vertically, and each PA-6 chain contains 10 monomer units. The linear dimension of the simulation domain is 1270 Å × 1270 Å × 49 Å with 8.7×10^6 atoms in total. AIREBO and DREIDING potentials are used for graphene and PA-6, respectively [16,17]. Non-equilibrium MD is employed to investigate the thermal behavior of the system. The method is dedicated to obtaining the steady-state temperature field under constant heat flux [18,19]. Specifically, by installing a heat source and a heat sink on opposite sides, the simulation domain will eventually reach a steady state after sufficient MD steps, as shown in Figure 1b. The effective thermal conductivity of the simulation domain can be easily calculated via Fourier's law.

Although molecular dynamics (MD) simulations can determine the transport properties of multiphase materials with high fidelity, they are computationally prohibitive. For example, the case considered here requires more than 1000 CPU cores running for approximately two weeks to approach steady state. To reduce this cost, we extract the key microstructural features of the original configuration and represent them as anisotropic, homogenized cells that can be efficiently treated within a continuum-scale finite element framework. As illustrated in Figure 1c,d, the original domain comprises three primary features, i.e., the pure PA-6 matrix, graphene segments, and inter-graphene contacts, which are correspondingly mapped to three types of lattice cells. The transport behaviors of the cells are determined by four parameters, i.e., κ_m, $\kappa_{\parallel}$, $\kappa_{\perp}$, and κ_t, which are for the transport efficiencies of the polymeric matrix, the graphene sheet, the polymer–graphene interface, and the inter-graphene contact. Properly adjusting these parameters, we can accurately reproduce the MD simulation result by performing FEM on the lattice model shown in Figure 1e. By setting $\kappa_m = 0.42\ W \cdot m^{-1} \cdot K$, $\kappa_{\parallel} = 6.9\ W \cdot m^{-1} \cdot K$, $\kappa_{\perp} = 0.4\ W \cdot m^{-1} \cdot K$, and $\kappa_t = 5.0\ W \cdot m^{-1} \cdot K$, Figure 1f compares the vertical temperature profiles obtained by FEM and MD, which are in perfect agreement. These parametric values are obtained by calibrating the temperature distribution obtained from the lattice-based FEM model with that from the non-equilibrium molecular dynamics simulation. The final parameter set was selected when the continuum lattice model accurately reproduced the MD temperature profile.

The above numerical experiment suggests that the lattice of the abstracted cells can be used to efficiently investigate the multiphase transport behaviors. Based on this, we introduce the following strategy to generate lattice models for composite media of arbitrary filler configurations and transport parameters. Starting from a domain purely consisting

of matrix cells, the second phase is seeded by randomly flipping some matrix cells, which are iteratively expanded either in the horizontal or vertical direction for a total of λ_m steps. Specifically, at the expansion step λ, all the filler particles grow by one lattice constant, and an inter-particle junction cell forms if two expanding filler particles come into contact. Topological percolation occurs when the maximally connected filler cluster spans across the entire domain. Denoting the number of filler particles within the maximally connected cluster by $\mathcal{S}$, Figure 2a,b demonstrate the evolution of the lattice configurations and the topological percolation transition during the expansion process.

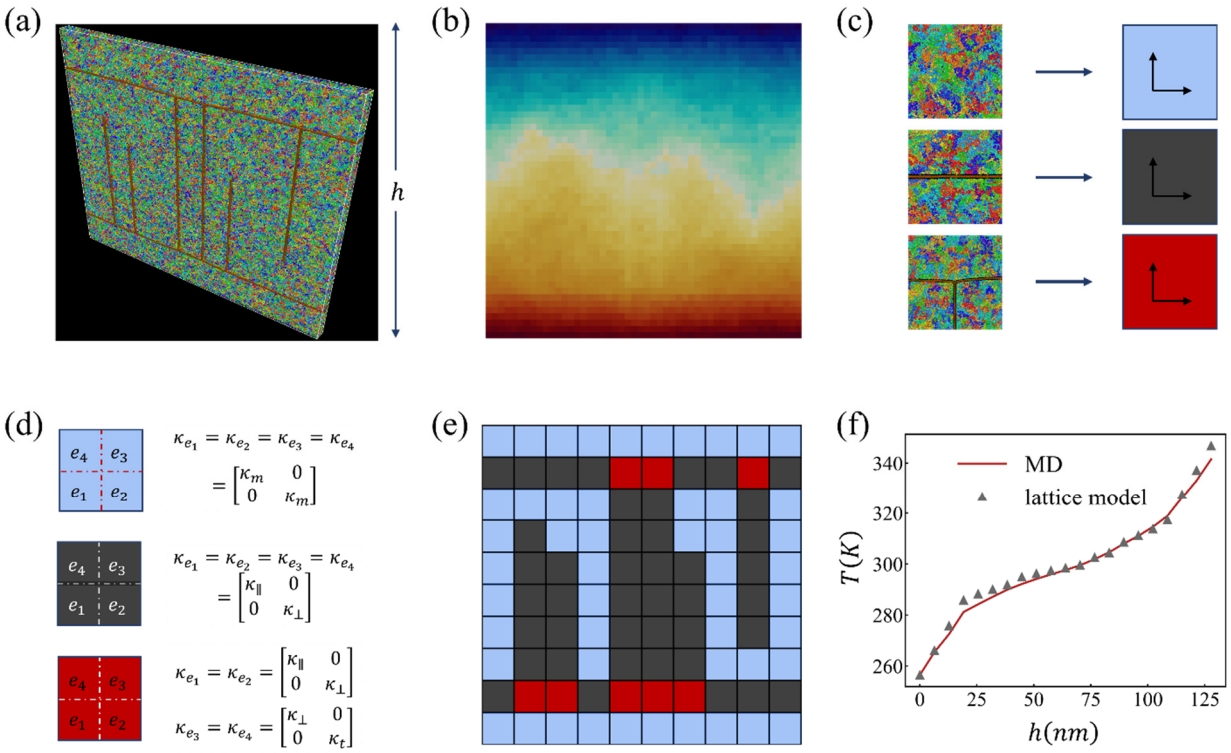

Figure 1. (**a**) The atomic configuration of the graphene-reinforced PA-6 composite material. Here, the brown stripes are the graphene flakes whose out-of-plane thickness is 49 Å, and the remainder is the matrix of PA-6 chains. (**b**) The obtained steady-state temperature field obtained by non-equilibrium MD simulation. (**c**) The extractions of the microstructural features from the original composite configuration. Again, the brown stripes are the graphene flakes while the remainder is the PA-6 matrix. (**d**) The assignment of transport parameters for the lattice cells. (**e**) The assembled lattice model for the original composite material. (**f**) Comparison of the vertical temperature profiles obtained from the lattice model and the molecular simulation. The vertical temperature profile is calculated by averaging the steady-state temperature field along the horizontal dimension.

For each lattice configuration, we can simulate different transport behaviors by varying the physical parameters of the lattice cells. For convenience, we assume that all the physical variables are in consistent units and the linear dimension of the lattice model is 1×1. The steady-state transport behavior is governed by a universal differential equation $\boldsymbol{q} = \boldsymbol{\rho} \nabla p$, generalized from Ohm's law and Fourier's law, where p represents the responsive field (temperature or electrical potential), $\boldsymbol{q}$ is the flux field (heat flux or electrical current density), and $\boldsymbol{\rho}$ is the tensor of transport property (thermal conductivity or electrical conductivity). To determine the overall transport property, we set constant responsive field value $p_t = 2$ to the top end and $p_b = 1$ to the bottom end of the lattice model and use FEM to calculate the corresponding p and $\boldsymbol{q}$ fields. The obtained steady-state fields are shown in Figure 2c,d,

from which the effective transport property along the vertical direction, denoted by $\overline{\rho}$, can be easily calculated via $\overline{\rho} = \left|\overline{q_y}\right|(p_t - p_b)^{-1}$.

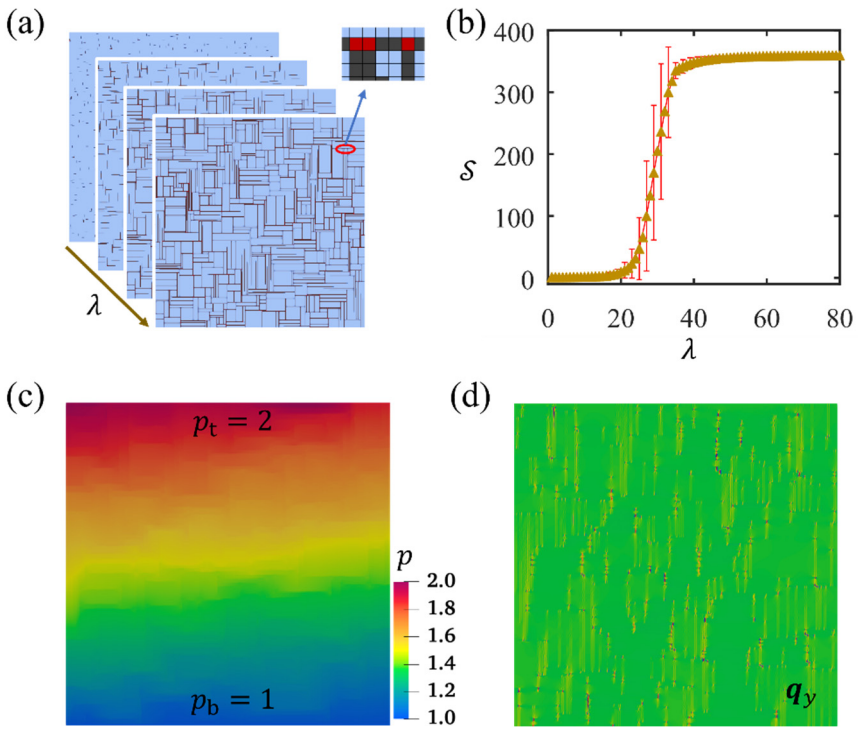

Figure 2. (**a**) The lattice models obtained at different expansion steps. (**b**) The size evolution of the maximally connected filler cluster (or the giant component) during the expansion process, where a clear topological percolation can be observed. (**c**,**d**) The steady-state responsive field p (can be temperature or electric potential) and flux field $\boldsymbol{q}_y$ (can be heat flux or current density) calculated by applying FEM to each of the lattice models.

3. Data-Driven Analysis of the Transport Behaviors

Equipped with the computationally efficient lattice model, we can efficiently gather the transport behaviors of multiphase configuration and flexibly set the physical parameters for the constituent phases. Now that the initial parameters of κ_m, $\kappa_{\parallel}$, $\kappa_{\perp}$ and κ_t have accurately reproduced graphene/PA-6, for the subsequent study, our goal is to explore the general transport behavior of heterogeneous composite media, instead of accurately reproducing a specific material system. Therefore, κ_m and $\kappa_{\parallel}$ will be fixed as reference values, while the transport efficiencies of the particle–matrix interface $\kappa_{\perp}$ and the inter-particle contact κ_t will be systematically varied over broad ranges to identify the controlling factors for transport percolation.

To start with, we generate a series of lattice models whose filler phase ranges from sparsely dispersed to topologically percolated as λ increases from 1 to 200. For each lattice model, the physical parameters of its lattice cells are sampled from some predefined ranges and the effective transport property $\overline{\rho}$ is determined by FEM. Specifically, we assume that the intrinsic transport properties of the matrix and the second phase are fixed, i.e., $\kappa_m = 1$ and $\kappa_{\parallel} = 10^3$, and we define two dimensionless variables, $\beta = \frac{\kappa_{\perp}}{\kappa_m}$ and $\gamma = \frac{\kappa_t}{\kappa_m}$, as the controlling parameters of $\kappa_{\perp}$ and κ_t. For the parametric sweep study, β is logarithmically sampled from the range $\left[10^{-5}, 10^{1}\right]$ and γ from $\left[10^{-1}, 10^{4}\right]$. Although more extreme values for these parameters might be encountered in reality, we cannot explore such scenarios with FEM due to the degradation of the global stiffness matrix and the numerical stability issue that comes with it. Figure 3a demonstrates the FEM-calculated $\overline{\rho}$ vs. λ curves under various $\{\beta, \gamma\}$.

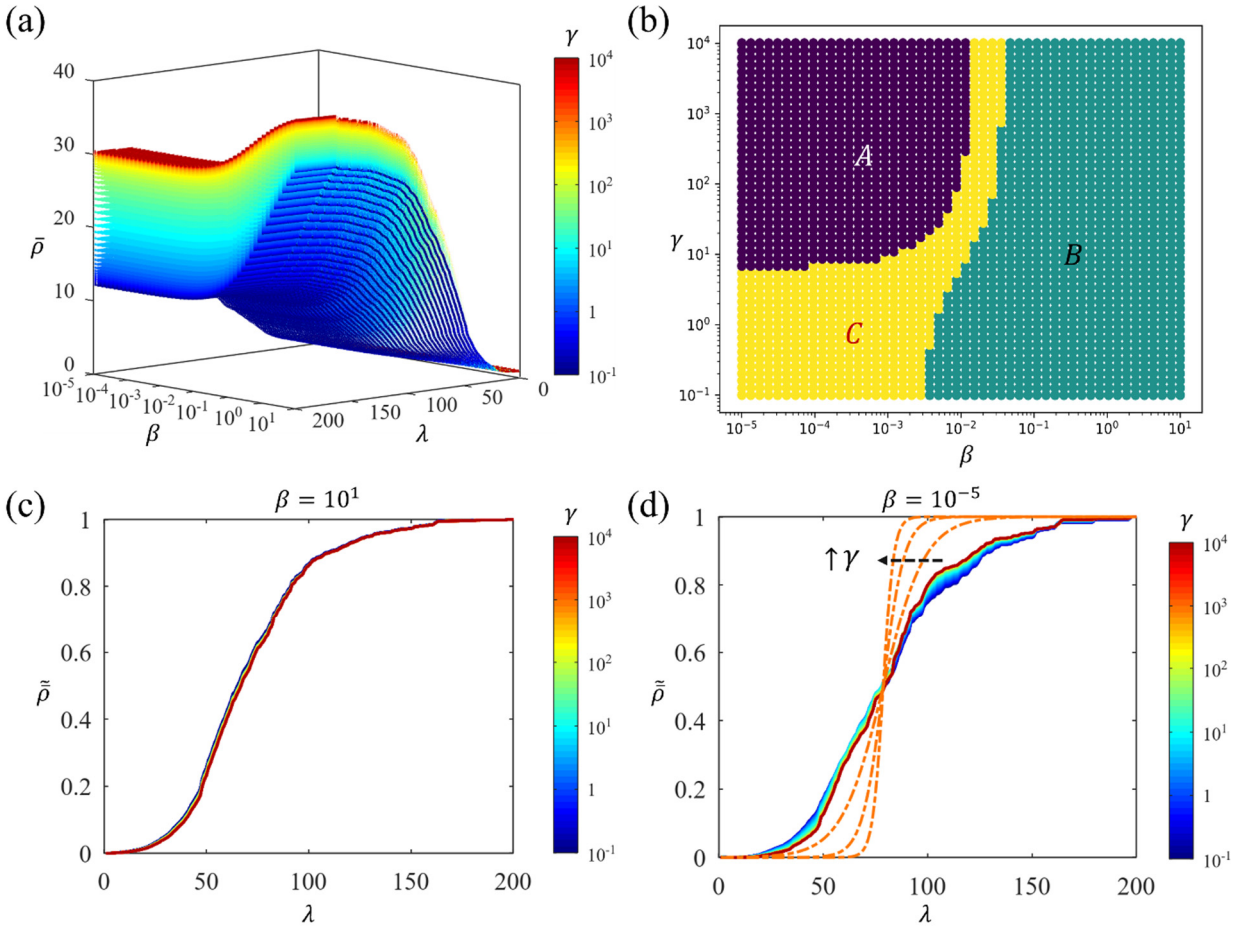

Figure 3. (**a**) The FEM results of the effective transport property $\overline{\rho}$ under different λ, β, and γ. (**b**) The data-driven partition of the $\beta - \gamma$ space according to the characteristics of the $\overline{\rho}$ vs. λ curves. (**c**,**d**) The normalized effective transport property $\widetilde{\overline{\rho}}$ vs. λ for $\beta = 10^1$ and $\beta = 10^{-5}$, respectively. The curves are colored by the value of γ. Note that $\beta = \frac{\kappa_\perp}{\kappa_m}$ and $\gamma = \frac{\kappa_t}{\kappa_m}$.

A data-driven framework is constructed to learn from the FEM results and automatically detect the similarities within the gathered dataset. First, an autoencoder module is introduced to extract the key features of ρ vs. λ curves [20]. Then, the unsupervised K-means method is used to pre-categorize the feature space into a few groups and output the centroid of each group [21]. Next, the resulting centroids are passed to the t-SNE classification model as the initial seeds, and the t-SNE module further analyzes the low-dimensional feature space and generates a confusion matrix [22]. Finally, the $\beta - \gamma$ space is partitioned into distinct regions according to the confusion matrix. Figure 3b demonstrates the classification results where three categories are obtained through this data-driven process. In particular, regions A and B correspond to the scenarios when the interfacial transport efficiency $\kappa_\perp$ is small and large, while region C can be regarded as the blurred boundary between A and B. This classification map suggests that β can be a critical indicator parameter which can distinguish different types of transport behaviors.

Although the data-driven analysis has automatically partitioned the transport behaviors into two major types, we are still not clear on how they are related to the percolation-absence and percolation-presence transport behaviors. To analyze the $\overline{\rho}$ vs. λ curves on the same grounds, we normalize all the $\overline{\rho}$ vs. λ curves into the same range. Denoting the effective transport property at the final expansion step λ_m by $\overline{\rho}_{\lambda_m}$, we introduce the normalized effective transport property $\widetilde{\overline{\rho}}$, which is obtained via $\widetilde{\overline{\rho}} = \overline{\rho}\,\overline{\rho}_{\lambda_m}^{-1}$. Figure 3c,d

demonstrate $\widetilde{\overline{\rho}}$ vs. λ for $\beta = 10^1$ and 10^{-5}, respectively. For the former scenario, we can see that all the $\widetilde{\overline{\rho}}$ vs. λ curves collapse to the same pattern regardless of the magnitude of γ. This means that, no matter how one improves the transport efficiency of the filler network, the pattern of the $\overline{\rho}$ vs. λ curve remains unchanged, which excludes the possibility of transport percolation. For the latter scenario, we find that the $\widetilde{\overline{\rho}}$ vs. λ curve gradually approaches the topological percolation curve as γ increases. Following this trend, as long as the transport efficiency of the filler cluster is sufficiently large, the $\overline{\rho}$ vs. λ would eventually exhibit a percolation transition. Therefore, regions A and B correspond to the scenarios where transport percolation is allowed and prohibited, respectively.

The above results indicate that the interfacial conductivity, $\kappa_\perp$, between the matrix and the filler is the primary factor governing the emergence of transport percolation. But counterintuitively, lower values of $\kappa_\perp$ correspond to a higher likelihood of percolation. From a physical perspective, β quantifies the efficiency of transport across the filler–matrix interface relative to transport through the matrix itself. To connect this computational parameter to measurable physical quantities and microscopic mechanisms, we must consider the distinct physics governing thermal and electrical transport at nanoscale interfaces. For thermal transport, the perpendicular interfacial conductivity $\kappa_\perp$ is fundamentally limited by Kapitza resistance (R_K thermal boundary resistance) at filler–matrix interfaces [23], which arises from phonon scattering due to acoustic impedance mismatch. R_K is usually of the same magnitude as the thermal resistance of the matrix, as in graphene-reinforced polymer composites, resulting in relatively large β. Moreover, the mechanical and thermal coupling at the inter-filler contact is largely suppressed when the contact is not perfectly coordinated, resulting in small γ. Therefore, the thermal conduction in graphene-reinforced polymer composites usually ends up in region B on the percolation diagram, where transport percolation is less likely to occur.

For electrical transport in composites with insulating polymer matrices, the situation is fundamentally different due to the quantum mechanical phenomenon of electron tunneling [24]. When conductive fillers are separated by nanometer-scale polymer gaps (typically < 5 nm), electrons can tunnel through the insulating barrier without requiring direct physical contact. This tunneling conductance depends exponentially on the gap distance and the barrier height, effectively extending the interaction radius of each filler particle and dramatically lowering the apparent electrical percolation threshold below the geometric contact threshold [25]. In the context of our lattice model, tunneling-enhanced electrical conduction corresponds to an effectively large contact conductivity $\gamma = \kappa_t/\kappa_m$ even in the absence of direct filler–filler contact. Meanwhile, the electrical conductance between the insulating matrix and conducting filler is zero, resulting in $\beta = 0$. Therefore, the electrical conduction in graphene-reinforced polymer composites ends up in region A on the diagram, corresponding to the percolation-allowed scenario.

It needs to be clarified that the phase boundary identified in this work is largely derived from computational modeling. A rigorous validation of this boundary would require accurate characterization of both the electrical conductivity of the matrix–filler interface and the contact conductance between adjacent fillers. To the best of our knowledge, obtaining such measurements remains extremely challenging using either molecular dynamics simulations or experimental techniques. Consequently, a direct validation of our findings is not feasible at the present stage due to a lack of accurately measured parameter values. Nevertheless, the clear physical meaning of parameters β and γ still helps us to understand the possible origin of the distinction between electrical percolation and thermal percolation.

Although the lattice model is inspired by the graphene/PA-6 composite, the proposed framework is not specific to this composite system. The key parameters in our model, β and γ, represent the relative interfacial transport efficiency and inter-filler junction trans-

port efficiency, respectively, which are general descriptors of heterogeneous transport behavior. Previous experimental observations of readily observable electrical percolation and the absence of conclusive evidence for thermal percolation in graphene/polymer and carbon nanotube/polymer composites are in good agreement with the general physical mechanism predicted by the $\beta - \gamma$ phase diagram developed in this work.

Of course, real composite materials have many other factors that may influence the above phase diagram. For example, size distribution, orientation distribution, and dimensionality of the reinforcement particles may all have certain effects. However, these factors only influence on the geometric percolation behavior of the reinforcement particles, which is a prerequisite of the transport percolation that we are focused on here. Therefore, these extra factors usually only affect the location of the phase boundary. Similarly, for three-dimensional composites with fillers of different shapes and orientations, the same principle is expected to apply because transport percolation is still governed by the competition between filler connectivity and interfacial transport resistance. Nevertheless, the exact phase boundary may shift depending on filler geometry, orientation distribution, and three-dimensional interface structures. Extending the present model to fully three-dimensional architectures with arbitrary reinforcement particle size and orientation distributions is an important direction for future work.

4. Numerical Singularity as Indicator for Transport Percolation

Up to now, the transition from non-percolative transport to percolative transport is still not a well-defined criticality. However, we find some interesting numerical singularities in the percolative transport regime. Figure 4a presents a mini-lattice model where the filler network spans across the entire domain, a feature of topologically percolated configuration. We pick a parametric set from each of region A and region B to inspect the difference between percolation-allowed and percolation-prohibited transport behavior. Figure 4b demonstrates the contour plot of the steady-state temperature field with $\beta = 1, \gamma = 10^4$ (a point from region A), while Figure 4c presents the result for $\beta = 10^{-2}, \gamma = 10^4$ (a point from region B). Different from the first case, we can easily find that some isolines near the matrix–filler interface form loops in the second case. The loops in the contour plot indicate that the interfacial flux exchange is chaotic. From a physical perspective, this can be explained by the fact that when the interfacial conductivity $\kappa_\perp$ (or β) is sufficiently low, the matrix–filler flux exchange is numerically instable, so the matrix phase and the filler phase become thermally decoupled. As a result, below the topological percolation, the matrix phase is the only transport carrier; above the topological percolation, the filler phase is the only transport carrier, as depicted in Figure 4d. Only under such circumstances does the transport percolation become well-defined. Therefore, the numerical instability here can be used as a criterion for the occurrence of transport percolation.

In fact, such numerical instability in the transport percolation regime is not unique to FEM. Figure 4e investigates the thermal transport behavior of a small piece of the graphene-reinforced PA-6 composite via non-equilibrium MD simulation. Figure 4f presents the steady-state temperature profile (obtained from extended MD simulations continued until no appreciable temperature variation is observed anywhere within the domain) along the vertical direction. It can be seen that there is also a contradictory temperature distribution within the vicinity of location h_X. Since the temperature on the graphene at location h_X is higher than the temperature on the PA-6 matrix above it, there should be heat flux going from the graphene at h_X to the upper PA-6 matrix. Noting that the heat flux is applied from the top to the bottom, the region Ω depicted in Figure 4e should accept heat flux from both directions and continue to heat up. But in reality, the temperature in the domain no longer changes, even under prolonged MD steps. Such contradiction indicates that the thermal

exchange between graphene and PA-6 at h_X is chaotic, similar to in Figure 4c. This, again, suggests that the numerical instability within the interfacial area can be a criterion for transport percolation. Only when the interface flux exchange is negligible is the transport percolation well-defined and in alignment with the topological percolation.

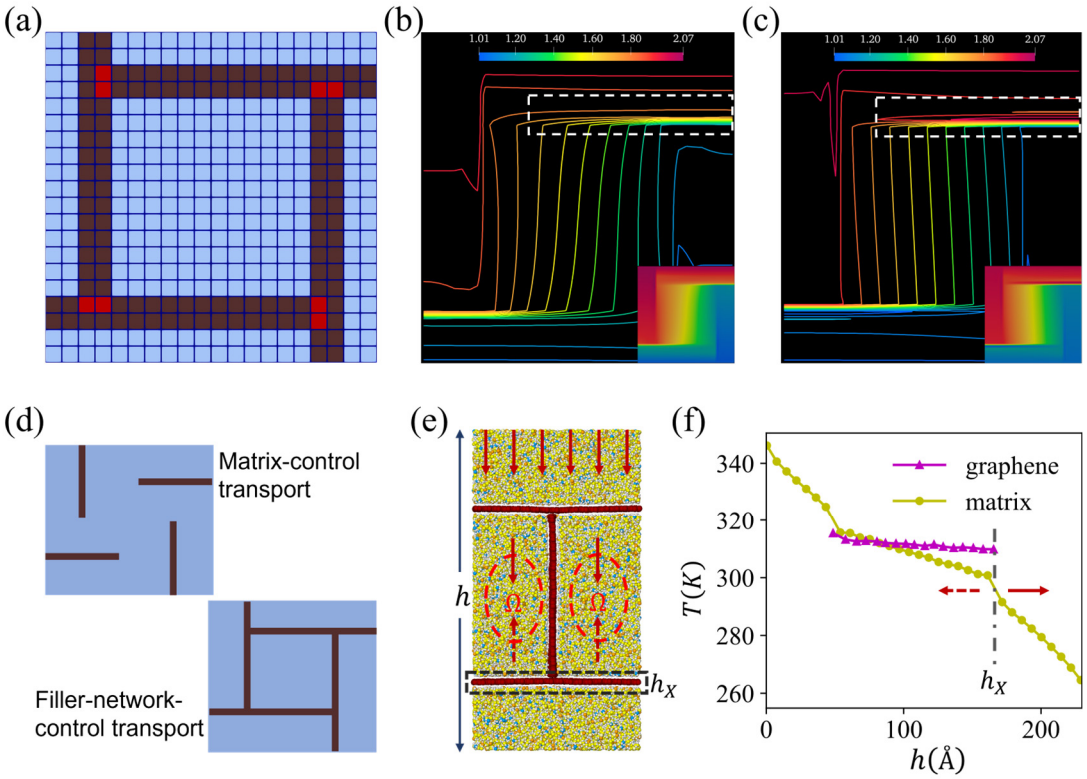

Figure 4. (**a**) A meshed mini-sample of the lattice model. (**b**,**c**) The steady-state responsive fields and corresponding contours for $\{\beta = 1, \gamma = 10^4\}$ and $\{\beta = 10^{-2}, \gamma = 10^4\}$, respectively. The white dashed boxes point out where the numerical instability occurs. (**d**) The extracted responsive field values along the dashed lines in (**b**,**c**). The highlighted spike represents the pseudo-source. (**e**) The atomic configuration of a mini-sample of the graphene-reinforced PA-6 composite. The red dashed region points out where the contradiction occurs. (**f**) The steady-state temperature profiles along the vertical direction calculated for the PA-6 matrix and graphene, respectively. Note that the temperature on the graphene at h_X is higher than the PA-6 matrix below and above, suggesting that heat flux should flow both downward and upward. The solid arrow shows the actual heat flow, while the dashed arrow represents the expected heat flow due to the temperature gradient—yet it is not actually present.

5. Conclusions

In sum, the emergence of transport percolation in multiphase medium is mainly controlled by the transport conductivity of the interface among the constituent phases. When the interfacial transport conductivity is not negligible, the flux can go continuously through the interface of phases and prohibit the occurrence of abrupt transport behavior upon topological percolation. Under this circumstance, the effective conductivity of the composite can be handled by the effective medium theory, which results in a smooth dependence of the effective transport property on the fraction of the second-phase fillers, eliminating the possibility of transport percolation. When the interfacial transport conductivity is sufficiently small that numerical instability occurs within the interfacial area, the flux is strongly impeded by the matrix–filler interface, making the matrix and the second phase practically decoupled. As a result, below the topological percolation, the matrix phase is continuous while the second-phase fillers do not form a spanning network, so

the transport process is entirely controlled by the matrix phase. Above the topological percolation, the second-phase fillers become a giant spanning network while the matrix phase is fragmented, so the transport process is entirely controlled by the filler phase. The interfacial conductivity, the transport percolation map, and the identified numerical singularity provide a useful framework for understanding the role of interfacial transport in macroscopic transport percolation. Further incorporation of geometric and structural factors may enable more comprehensive prediction of transport percolation in complex heterogeneous materials.

Author Contributions: Conceptualization, S.C. and N.X.; methodology, S.C.; software, H.W.; validation, S.C., H.W. and N.X.; formal analysis, S.C.; investigation, S.C. and H.W.; resources, S.C. and N.X.; data curation, H.W.; writing—original draft preparation, S.C. and N.X.; writing—review and editing, S.C. and N.X.; supervision, N.X.; project administration, N.X.; funding acquisition, S.C. and N.X. All authors have read and agreed to the published version of the manuscript.

Funding: This work is funded by the National Natural Science Foundation of China (No. 12302178, 12402162), the Natural Science Foundation of Jiangsu Province (No. BK20230897), the Key Laboratory of Inlet and Exhaust Technology, Ministry of Education (No. CEPE2024010), and China Post-Doctoral Research Foundation (Grant No. 2025M771863).

Institutional Review Board Statement: Not applicable.

Informed Consent Statement: Not applicable.

Data Availability Statement: The data that support the findings of this study are available from the corresponding author upon reasonable request. The data are not publicly available due to legal and institutional restrictions.

Conflicts of Interest: The authors declare no conflicts of interest.

References

1. Manfra, M.J.; Hwang, E.H.; Das Sarma, S.; Pfeiffer, L.N.; West, K.W.; Sergent, A.M. Transport and Percolation in a Low-Density High-Mobility Two-Dimensional Hole System. *Phys. Rev. Lett.* **2007**, *99*, 236402. [CrossRef] [PubMed]
2. McLachlan, D.S. The percolation exponents for electrical and thermal conductivities and the permittivity and permeability of binary composites. *Phys. B Condens. Matter* **2021**, *606*, 412658. [CrossRef]
3. Shtein, M.; Nadiv, R.; Buzaglo, M.; Kahil, K.; Regev, O. Thermally Conductive Graphene-Polymer Composites: Size, Percolation, and Synergy Effects. *Chem. Mater.* **2015**, *27*, 2100–2106. [CrossRef]
4. Li, A.; Zhang, C.; Zhang, Y.-F. Graphene nanosheets-filled epoxy composites prepared by a fast dispersion method. *J. Appl. Polym. Sci.* **2017**, *134*, 45152. [CrossRef]
5. Shahil, K.M.F.; Balandin, A.A. Graphene–Multilayer Graphene Nanocomposites as Highly Efficient Thermal Interface Materials. *Nano Lett.* **2012**, *12*, 861–867. [CrossRef] [PubMed]
6. Hu, L.; Desai, T.; Keblinski, P. Thermal transport in graphene-based nanocomposite. *J. Appl. Phys.* **2011**, *110*, 3. [CrossRef]
7. Huang, J.; Zhu, Y.; Xu, L.; Chen, J.; Jiang, W.; Nie, X. Massive enhancement in the thermal conductivity of polymer composites by trapping graphene at the interface of a polymer blend. *Compos. Sci. Technol.* **2016**, *129*, 160–165. [CrossRef]
8. Maruzhenko, O.; Mamunya, Y.; Boiteux, G.; Pusz, S.; Szeluga, U.; Pruvost, S. Improving the thermal and electrical properties of polymer composites by ordered distribution of carbon micro- and nanofillers. *Int. J. Heat Mass Transf.* **2019**, *138*, 75–84. [CrossRef]
9. Vu, M.C.; Choi, W.K.; Lee, S.G.; Park, P.J.; Kim, D.H.; Islam, M.A.; Kim, S.R. High Thermal Conductivity Enhancement of Polymer Composites with Vertically Aligned Silicon Carbide Sheet Scaffolds. *ACS Appl. Mater. Interfaces* **2020**, *12*, 23388–23398. [CrossRef] [PubMed]
10. Shenogina, N.; Shenogin, S.; Xue, L.; Keblinski, P. On the lack of thermal percolation in carbon nanotube composites. *Appl. Phys. Lett.* **2005**, *87*, 133106. [CrossRef]
11. Lasance, C.J.M. Ten Years of Boundary-Condition- Independent Compact Thermal Modeling of Electronic Parts: A Review. *Heat Transf. Eng.* **2008**, *29*, 149–168. [CrossRef]
12. Sarikhani, N.; Arabshahi, Z.S.; Saberi, A.A.; Moshfegh, A.Z. Unified modeling and experimental realization of electrical and thermal percolation in polymer composites. *Appl. Phys. Rev.* **2022**, *9*, 041403. [CrossRef]

13. Forero-Sandoval, I.Y.; Franco-Bacca, A.P.; Cervantes-Álvarez, F.; Gómez-Heredia, C.L.; Ramírez-Rincón, J.A.; Ordonez-Miranda, J.; Alvarado-Gil, J.J. Electrical and thermal percolation in two-phase materials: A perspective. *J. Appl. Phys.* **2022**, *131*, 230901. [CrossRef]
14. Stankovich, S.; Dikin, D.A.; Dommett, G.H.; Kohlhaas, K.M.; Zimney, E.J.; Stach, E.A.; Piner, R.D.; Nguyen, S.T.; Ruoff, R.S. Graphene-based composite materials. *Nature* **2006**, *442*, 282–286. [CrossRef] [PubMed]
15. Chen, S.; Liu, Q.; Gorbatikh, L.; Seveno, D. Does Thermal Percolation Exist in Graphene-Reinforced Polymer Composites? A Molecular Dynamics Answer. *J. Phys. Chem. C* **2021**, *125*, 1018–1028. [CrossRef]
16. Stuart, S.J.; Tutein, A.B.; Harrison, J.A. A reactive potential for hydrocarbons with intermolecular interactions. *J. Chem. Phys.* **2000**, *112*, 6472–6486. [CrossRef]
17. Mayo, S.L.; Olafson, B.D.; Goddard, W.A. DREIDING: A generic force field for molecular simulations. *J. Phys. Chem.* **1990**, *94*, 8897–8909. [CrossRef]
18. Evans, D.J. Homogeneous NEMD algorithm for thermal conductivity—Application of non-canonical linear response theory. *Phys. Lett. A* **1982**, *91*, 457–460. [CrossRef]
19. Barbarino, G.; Melis, C.; Colombo, L. Intrinsic thermal conductivity in monolayer graphene is ultimately upper limited: A direct estimation by atomistic simulations. *Phys. Rev. B* **2015**, *91*, 035416. [CrossRef]
20. Baldi, P. Autoencoders, Unsupervised Learning, and Deep Architectures. In *Proceedings of the ICML Workshop on Unsupervised and Transfer Learning*; JMLR Workshop and Conference Proceedings: Bellevue, WA, USA, 2012; pp. 37–49. Available online: http://proceedings.mlr.press/v27/baldi12a.html (accessed on 22 July 2026).
21. MacQueen, J. Some Methods for Classification and Analysis of Multivariate Observations. In *Proceedings of the Fifth Berkeley Symposium on Mathematical Statistics and Probability, Volume 1: Statistics*; University of California Press: Oakland, CA, USA, 1967; pp. 281–298.
22. Hinton, G.E.; Roweis, S. Stochastic Neighbor Embedding. In *Advances in Neural Information Processing Systems*; MIT Press: Cambridge, MA, USA, 2002; Volume 15. Available online: https://proceedings.neurips.cc/paper_files/paper/2002/hash/6150ccc6069bea6b5716254057a194ef-Abstract.html (accessed on 22 July 2026).
23. Hu, X.F.; Yao, W.A.; Yang, S.T. A Symplectic Analytical Singular Element for Steady-State Thermal Conduction with Singularities in Anisotropic Material. *J. Heat Transf.* **2018**, *140*, 091301. [CrossRef]
24. Gau, C.; Kuo, C.-Y.; Ko, H.S. Electron tunneling in carbon nanotube composites. *Nanotechnology* **2009**, *20*, 395705. [CrossRef] [PubMed]
25. Haghgoo, M.; Ansari, R.; Hassanzadeh-Aghdam, M.K.; Nankali, M. Analytical formulation for electrical conductivity and percolation threshold of epoxy multiscale nanocomposites reinforced with chopped carbon fibers and wavy carbon nanotubes considering tunneling resistivity. *Compos. Part A Appl. Sci. Manuf.* **2019**, *126*, 105616. [CrossRef]